IEEE Access
Multidisciplinary : Rapid Review : Open Access Journal

Received 8 August 2023, accepted 5 October 2023, date of publication 10 October 2023, date of current version 16 October 2023.

Digital Object Identifier 10.1109/ACCESS.2023.3323250

RESEARCH ARTICLE

Functional Brain Network Measures for Alzheimer's Disease Classification

LUYUN WANG[1,2,3], JINHUA SHENG[1,2], (Senior Member, IEEE), QIAO ZHANG[4,5], ROUGANG ZHOU[2,6,7], ZHONGJIN LI[1,2], YU XIN[1,2], AND QIAN ZHANG[1,2]

[1]School of Computer Science and Technology, Hangzhou Dianzi University, Hangzhou, Zhejiang 310018, China
[2]Key Laboratory of Intelligent Image Analysis for Sensory and Cognitive Health, Ministry of Industry and Information Technology of China, Hangzhou, Zhejiang 310018, China
[3]Hangzhou Vocational and Technical College, Hangzhou, Zhejiang 310018, China
[4]Beijing Hospital, Beijing 100730, China
[5]Institute of Geriatric Medicine, Chinese Academy of Medical Sciences, Beijing 100730, China
[6]College of Mechanical Engineering, Hangzhou Dianzi University, Hangzhou, Zhejiang 310018, China
[7]Mstar Technologies Inc., Hangzhou, Zhejiang 310018, China

Corresponding author: Jinhua Sheng (j.sheng@ieee.org)

This work was supported in part by the National Natural Science Foundations of China under Grant 62271177 and Grant 61871168, in part by the Zhejiang Provincial Natural Science Foundation of China under Grant LTGY23F020004, in part by the General Scientific Research Projects of Zhejiang Education Department under Grant Y202148102, and in part by the Alzheimer's Disease Neuroimaging Initiative (ADNI).

ABSTRACT Background: Alzheimer's disease (AD) is an incurable neurodegenerative disease primarily affecting the elderly population. The therapy of AD depends heavily on an early diagnosis. In this study, our primary objective is to evaluate the classification framework, which combines graph theory and machine learning techniques for functional magnetic resonance imaging (fMRI), to distinguish AD, early mild cognitive impairment (EMCI), late mild cognitive impairment (LMCI), and healthy control (HC). Methods: A novel multi-feature selection method, incorporating the dual graph theoretical approach, is proposed for classification. This method utilizes three different feature selection methods after brain areas selection through graph-theory analyses in 96 subjects with brain parcellation by using the joint human connectome project multimodal parcellation (J-HCPMMP) of 180 areas per hemisphere. Results: The classification results show that the optimal features selected by the minimal redundancy maximal relevance (MRMR) based on support vector machine linear (SVM-linear) from graph measures for 36 areas of 360 areas. The classification accuracies for identifying HC vs. EMCI, HC vs. LMCI, HC vs. AD, EMCI vs. LMCI, LMCI vs. AD, and EMCI vs. AD, are 85.60%, 92.90%, 96.80%, 83.30%, 84.90% and 89.50%, respectively. Conclusion: The results indicate that the combination of graph measures and machine learning in fMRI connectivity analysis might be helpful for the diagnosis of AD, especially the use of local measures, which may better reflect functional changes in local brain regions because of cognitive impairment.

INDEX TERMS Alzheimer's disease, functional brain network measures, feature selection, classification, fMRI.

I. INTRODUCTION

Alzheimer's disease (AD) is the most common type of irreversible neurodegenerative disorder, which is characterized by progressive impairment of memory and other cognitive functions in elderly people worldwide [1]. Since Alzheimer's disease is facing great challenges in terms of treatment, early screening, early warning, and early treatment are of paramount importance for AD prevention and intervention. To intervene in the diagnosis and treatment of AD diseases earlier, the diagnosis and prediction of AD diseases have been studied from multiple perspectives of brain imaging, genetics, and pathology. The diagnostic specificity of the pathological hallmarks of AD leads to the elucidation of biomarkers with proposed progression patterns [2]. Consequently, it is of clinical importance to discover highly discriminative features

The associate editor coordinating the review of this manuscript and approving it for publication was Li He.

and to establish a robust classification mechanism for AD diseases, especially to provide early warning signals to AD patients.

Functional magnetic resonance imaging (fMRI) is an exciting non-invasive tool that measures changes in blood flow and oxygenation levels in Brain. In particular, fMRI can not only reflect the local spatial information about brain function, but also maintain detailed functional connectivity maps of the brain [3]. fMRI has been utilized to analyze AD and has revealed significant impairments in large-scale brain functional network [4]. The advances in graph theory and network neuroscience (i.e. the study of structure or function of the nervous system) offer an opportunity to study the process of brain abnormality in Alzheimer's disease because of the altered structural and functional connectivity architecture of the brain in those suffering from this disease [5], [6]. The combination of graph theory and fMRI has been able to be used as a disease biomarker, revealing the abnormal connection of the structure or functional network of various brain regions in the development of Alzheimer's disease [7], [8], [9]. Since most studies have motivated by the observation of abnormal and inconsistent brain connections, many recent studies [10], [11] have employed the development of a classification framework that combines functional brain networks and machine learning to classify individuals with MCI or AD. Zhang et al. [10] aimed to evaluate the classification framework with fMRI metrics to distinguish mild cognitive impairment non-converters (MCInc)/AD from MCI converters (MCIc) by using graph theory and machine learning. They found that in the classifications of MCIc vs. MCInc, and MCIc vs. AD achieved the accuracies of 84.71 and 89.80%. Raamana et al. [12] constructed the brain network based on the difference in cortical thickness, by using the graph measures including the average clustering coefficient, boundary number, and node degree, and employed the Bayes classifier to achieve the classification accuracy of 64% for MCIc vs. MCInc.

With the development of graph theoretical approaches with advanced machine learning methods, more researchers are using data-driven techniques to discover potential neuroimaging biomarkers that can automate the identification of brain diseases. Generally, there are at least two disadvantages in existing graph theory combine with machine learning methods for brain functional connectivity network analysis. 1) Previous studies [13], [14] usually utilize all nodes for feature selection and feeding them as embedding into the classifier, which would lead to feature redundancy. Some regions of interest (ROIs) are more informative than others in predicting brain disorders. 2) Existing studies [15], [16], [17] generally use the parcellation approaches (i.e., Anatomical Automatic Labelling (AAL) template, 264 putative function areas, Brodmann), which not provide more detailed and accurate brain region delineation for AD. Therefore, it is crucial to focus more on the node features corresponding to the ROIs that are more indicative.

The aim of this study is to distinguish different stages of AD using the multi-feature selection method, combining graph theoretical approach and machine learning methods, applied to the fMRI data with a brain parcellation based on the joint human connectome project multimodal parcellation (J-HCPMMP) approach. For this, we first employ J-HCPMMP approach to partition each brain into 360 areas for generating brain functional connectivity work. We then calculate the connectivity measures using the fMRI data from the four groups, and analyse the connectivity measures using network-based statistics (NBS) analysis to extract the key brain areas and calculate the local and global graph measures from the connectivity matrices. Then, after choosing the graph measures, we use the multi-feature selection based on three different algorithms (MRMR, sparse linear regression feature selection algorithms based on stationary selection (SS-LR), and Fisher Score (FS)) to select the best features. Here, we analyse the relationship between network characteristics with global and local measures. Finally, we use SVM with nested cross-validation to classify the sample into two classes (HC vs. EMCI, HC vs. LMCI, HC vs. AD, EMCI vs. LMCI, LMCI vs. AD, and EMCI vs. AD) with four situations, including local graph measures for 360 areas, local graph measures plus global graph measures for 360 areas, local graph measures for 36 areas, and global graph measures for 360 areas. According to our results, using graph measures in conjunction with a multi-feature selection approach based on fMRI connectivity analysis may help in the diagnosis of Alzheimer's disease. Overall, the contributions of our work are summarized as below:

1) To propose an effective method for classification with fMRI in different AD stages.

2) To propose a complete pre-processing pipeline for constructively extracting functional connectivity matrices from fMRI data by using fine brain parcellation approach.

3) To identify the multi-feature selection with dual graph theory and machine learning for accurately classifying and identifying the brain regions contributing to AD.

The structure of the remainder paper is as follows. Section II introduces the most relevant studies. In section III, the materials used in this study are presented. Section IV describes the methods employed. Section V shows the experimental results. Sections VI provides the discussions on the findings. We conclude this paper in section VII.

II. RELATED WORK

A. FUNCTIONAL MAGNETIC RESONANCE IMAGING

Functional magnetic resonance imaging is a commonly used non-invasive imaging technique that provides a neuropathological approach to studying the organization of the brain and its cognitive functions. It measures hemodynamic changes and aids in simulating the functional and structural mechanisms of brain [18]. Compared to other imaging modalities such as structural MRI and positron emission tomography (PET), fMRI specifically provides information on brain

functional connectivity between different regions. The study of functional connectivity in AD provides insights into the underlying pathophysiological processes and cognitive impairments associated with the disease. By analyzing patterns of connectivity between brain regions, researchers can identify aberrant connectivity patterns and potentially relate them to specific cognitive deficits observed in AD patients. Recent researches [19], [20] have demonstrated a strong correlation between behavioral characteristics and alterations in functional connectivity as measured by fMRI. These findings suggest that changes in functional connectivity patterns are associated with neural mechanisms underlying various behaviors.

B. GRAPH THEORY FOR BRAIN CONNECTIVITY ANALYSIS

With the development of complexity theory, the combination of graph theory and fMRI has been used as a disease biomarker, revealing the abnormal connection of the structure or functional network of various brain regions in the development of Alzheimer's disease [9], [21], [22]. The fMRI connectivity analysis has been utilized to detect alterations in the brain network characteristic in AD, early mild cognitive impairment (EMCI), late mild cognitive impairment (LMCI), and healthy control (HC). To disclose the topological structure of AD and give helpful information for precise categorization, several research on the development of the brain network and machine learning techniques based on fMRI have been conducted [8], [23], [24]. Gao et al. [25] used a visibility graph (VG) to construct time-dependent brain network as well as functional connectivity networks. They used the VG method to map the time series of individual brain regions into the network and studied the topological abnormalities of local complex networks, and found several abnormal brain regions, including the left insula, right posterior cingulate gyrus, and other cortical regions. This identified that there were significant differences of local brain region network on temporal characteristics indexes between AD and HC. Wang et al. [26] explored network functional connectivity with AD and mild cognitive impairment (MCI) in the default mode network (DMN) and dorsal attention network (DAN). They found that intra- and inter- network connectivity was impaired in AD. Golbabaei et al. [27] used local and global measures to assess the functional brain network of each subject. They discovered that the olfactory cortex, hippocampus, par hippocampal, amygdala, and superior parietal gyrus all showed lower node strength, local clustering coefficient, and local efficiency as well as increased local characteristic path length in AD patients. Uysal et al. [28] employed the method of constructing a brain function network, and they found that the betweenness centrality in the right inferior temporal gyrus and the nodal degree in the left middle temporal gyrus was different in distinguishing between EMCI and LMCI. Luo et al. [29] used graph theory to characterize the brain network abnormalities of AD and MCI with a Chinese brain template. Researchers found that altered graph metrics, including assortativity coefficient, nodal degree centrality, nodal clustering coefficient, nodal efficiency, and nodal local efficiency, reflected plasticity of the brain in AD and MCI as compared with HC. However, existing methods based on graph theory typically treat feature selection equally across all regions without considering some brain regions. Besides, they employ the coarse brain parcellation templates of ROI parcellation to construct brain connectivity networks, which lacks detailed spatial resolution and restrict the ability to analyze specific brain regions in detail. Both issues may lead to sub-optimal performance of Alzheimer's disease classification.

C. MACHINE LEARNING FOR CLASSIFICATION

With the development of neuroimaging and artificial intelligence techniques, many fMRI-based machine learning algorithms have been proposed to distinguish the different stages of AD and provide useful information for more accurate classification. Khazaee et al. [30] combined the graph theoretical approach with support vector machine (SVM) to study the brain network for rest-state fMRI (rs-fMRI) with MCI, AD, and HC. Based on a parcellation of 264 putative areas as well as the AAL template, they were able to accurately classify three groups (i.e., HC, MCI, and AD) with 88.4% accuracy using the optimal features extracted from the graph measures. Seyed et al. [31] used graph theory and machine learning approach to classify MCI-converted (MCI-C) from MCI-non converted (MCI-NC) with rs-fMRI features and achieved accuracies of 93%. Lama et al. [32] applied graph theory from fMRI features to discriminate AD, MCI, and HC using a linear support vector machine (LSVM), and regularized extreme learning machine (RELM). As a result of using RELM and LSVM, MCI vs. AD was classified with 93.86%, and AD vs. HC with 90.63%. Zhang et al. [33] investigated the efficacy of a classification framework to distinguish by using functional brain network of rs-fMRI. According to the classification findings, the feature chosen using MRMR (minimum redundancy maximal relevance) was the best, with an accuracy rate of 83.87% for both LMCI and EMCI. In conclusion, machine learning based on fMRI connectivity analysis can correctly diagnose AD, LMCI, EMCI, and HC by integrating graph theoretical methodologies of complex networks. To this end, we propose a multi-feature selection method Alzheimer's disease identification based on functional connectivity networks.

III. MATERIALS

A. DATA ACQUISITION

The brain MR imaging data of 96 subjects are collected from the Alzheimer's Disease Neuroimaging Initiative (ADNI) (http://adni.loni.usc.edu). Informed consent was obtained from the volunteers in accordance with the institutional review board policy. All methods are carried out in accordance with relevant guidelines and regulations. All experimental protocols are approved by the institutional

TABLE 1. Demographic information of studied subjects in dataset.

	HC	EMCI	LMCI	AD
Number	24	24	24	24
Age(mean±SD)	76.0 ± 3.8	75.6 ± 6.0	78.0 ± 9.1	76.3 ± 9.6
Male:Female	8:16	13:11	11:13	12:12

review board (IRB) at Hangzhou Dianzi University (IRB-2020001).

Data from 24 patients with AD (average age of 76.3 ± 9.6, 16 females), 24 patients with EMCI (average age 75.6 ± 6.0, 11 females), 24 patients with LMCI (average age 78.0 ± 9.1, 13 females), and 24 age-matched HCs (average age 76.0 ± 3.8, 12 females) from the ADNI are analyzed in this study. The detailed information of the dataset can be found in Table 1. The brain MR imaging data of 96 subjects are including T1w and T2w structure data, field mapping and resting state fMRI with eyes open.

All functional and structural MRI images are collected by scanning on a 3-T Philips scanner according to the ADNI acquisition protocol. Data from structural MRI are collected for each scanner to obtain multidimensional 3D gradient echo images (T1W-3D-MPRAGE) and volumetric 3D sagittal magnetization images. A SENSE DTI sequence is performed using the following parameters: 170 contiguous 1 mm slices; FOV = 256 × 256 mm; TR: 6.78 ms; TE: 3.14 ms. Functional MRI data are collected using a 3.0 Tesla field strength in the resting state of the subject, the imaging resolution is 64 × 64; slices is 6720.0; slice thickness is 3.3 mm; TR/TE: 3000/30.0 ms; flip angle = 80°.

B. DATA PREPROCESSING

We used a new J-HCPMMP method [34] to describe the cortical architecture, function, and connectivity, which can accurately identify AD and MCI patients at different stages. The HCP MMP [35] is based on surface-based registrations of multimodal MR acquisitions and a semi-automated neuroanatomical approach to delineate 180 areas per hemisphere. These areas are defined by sharp changes in cortical architecture, function, and connectivity in a group average of 210 healthy young adults. To register ADNI data into Connectivity Informatics Technology Initiative (CIFTI) space and parcellate brain areas with HCP MMP, the J-HCPMMP divides the human brain into 180 areas per hemisphere using multimodal cerebral cortical partition techniques and the HCPMMP atlas. The J-HCPMMP maps the non-HCP protocol ADNI data into the HCP CIFTI grey space using T1W and fMRI data, without T2W data. Several brain data processing toolkits are used in J-HCPMMP including FreeSurfer, fMRIprep, CIFTIFY and HCP minimal preprocessing pipeline. The brain structural data of T1w are preprocessed using the standard surface-based stream provided by FreeSufer 5.0. The brain cortices with smoothed, mid-thickness, pial and inflated are extracted and saved as GIFTI. And then fMRI and field map are pre-processed with fMRIprep. The cerebral cortex is registered into CIFTI grey space, CIFTI defined 91,282 standard grey-ordinates in which consists of 32,492 cortical vertices per hemisphere and 26,298 individual elements in 19 subcutaneous tissues and dividing the 32,492 vertices of cerebral cortex into 180 areas. The weighted brain connection matrix and the binary brain connectivity matrix are then created using all the fMRI data from these 360 areas. The 360 J-HCPMMP functional areas are based on functional brain network and thus may be more sensitive to brain function organization.

IV. METHODS

We attempt to deal with two challenging issues in brain connectivity network analysis, i.e., 1); how to make use of dual local and globe measures with fine brain parcellation templates; and 2) how to fuse the multi-feature selection methods and machine learning for Alzheimer's disease identification. We propose a multi-feature selection method, incorporating the dual graph theoretical approach, for classification with the J-HCPMMP brain parcellation.

The overall procedure of this study is illustrated in Figure 1. First, the fMRI data are pre-processed with four groups (i.e., HC, EMCI, LMCI and AD) and parcellated into 360 areas using J-HCPMMP. We examine how global and local measurements relate to network characteristic parameters with six globe and six local graph measures based on 360 areas. And then the NBS analysis is performed to find optimal areas with the most discriminative ability in classification of different stages of AD. Subsequently, the extracted connection matrix is used for analysis after selecting 36 areas with local measures. After the selection of the graph measures, the best features are then chosen using a multi-feature selection approach based on three separate algorithms (MRMR, SS-LR, and FS). As a result, statistical analysis of brain functions and above optimal features are performed for identifying HC vs. EMCI, HC vs. LMCI, HC vs. AD, EMCI vs. LMCI, LMCI vs. AD, and EMCI vs AD. In our classification study, we compare the performances of various classifiers, including SVM-linear [36], K-nearest neighbor (KNN) [37], Linear Discriminant Analysis (LDA), Convolutional Neural Network (CNN) [38], and Decision tree [39].

A. NETWORK CONSTRUCTION AND NETWORK MEASURES ANALYSIS

The fMRI features are constructed based on graph theory and the connectivity matrix, reflecting the state of brain connections through structural or functional topological associations [40]. We study the changes in brain areas in groups with cognitive impairments using functional brain network. Each brain area is defined as the node of the brain network, and the correlation coefficient of the fMRI time series between brain partitions as the weight of the graph edge between nodes to construct the brain connection network. Thus, for each subject, a 360 × 360 adjacency matrix is generated by computing the correlation coefficients between any two brain

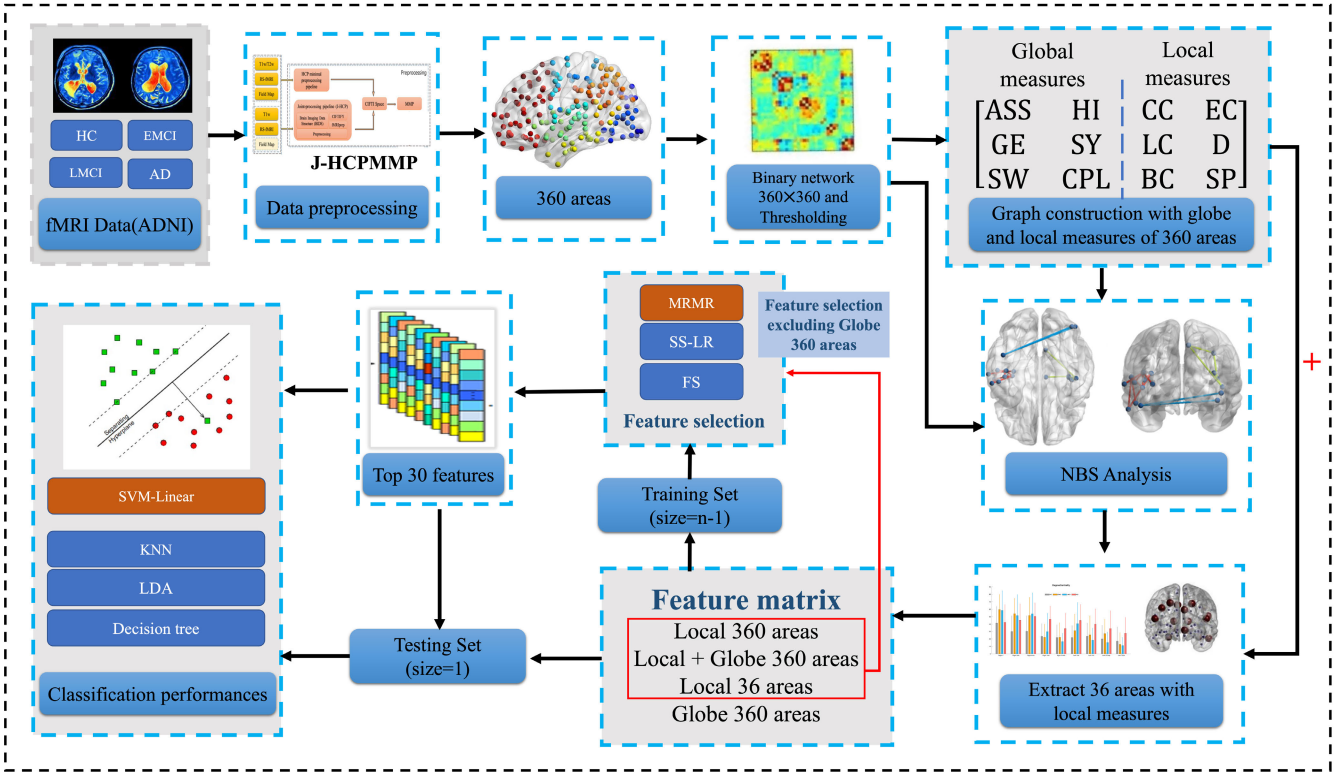

FIGURE 1. The overall procedure of functional network measures for classification.

areas, and the weights of all diagonals are set to 0. Then, both weighted and binary adjacent networks are produced using the proportion of the strong weights (PSW) [30] value to reduce noisy and weakly correlated connectivity. The brain connectivity matrix is sparsely processed using a data-driven PSW to maximize the global cost efficiency (GCE) in the brain connectivity matrix, as described in (1) and (2).

$$max_{PSW}(GCE) = E - PSW \tag{1}$$

$$E = \frac{1}{n}\sum_{i\in N} E_i = \frac{1}{n}\sum_{i\in N}\frac{\sum_{j\in N, j\neq i} d_{ij}^{-1}}{n-1} \tag{2}$$

where E_i is the efficiency of node i, n is the total number of nodes, N is the vector of all nodes, and d_{ij} is the shortest path length between node i and j. A range of candidate PSWs from 1% to 100% with a step of 1% is tested to maximize the GCE value.

When determining the strongest weight ratio, a sparse brain connectivity matrix is obtained. As part of the functional complex brain network, only functional connections between undirected brain areas of the brain are considered. Therefore, the absolute values of all correlation coefficients in the network are taken to remove negative correlations. Finally, the weighted network and the binary undirected network with node connection information is retained (Figure 2).

Various network measures are computed for the network of each subject. There are many measures for complex brain network, which can be divided into global network measures, local network measures, and small-world characteristics measures of brain connectivity [41]. The Brain Connectivity Toolbox (BCT toolbox) (https://sites.google.com/site/bctnet/) is

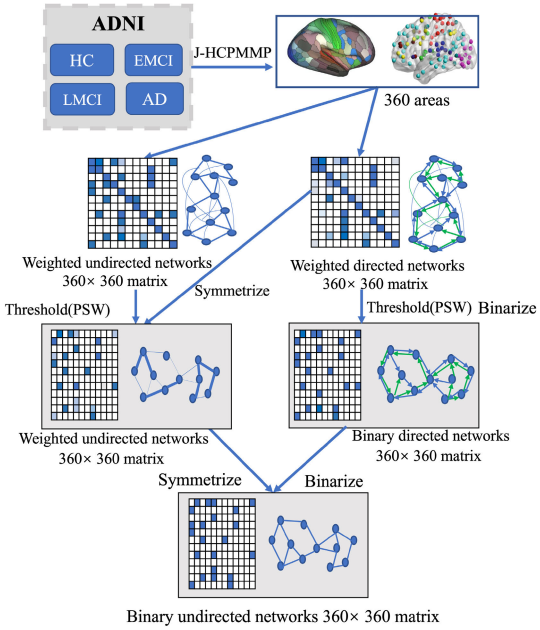

FIGURE 2. Construction of brain network from functional connectivity datasets.

employed to compute 6 local graph measures and 6 global graph measures. There are 360 graph nodes in this study. As a result, features for the following global measures are calculated for Assortativity (ASS), Globe Efficiency (GE), Small World (SW), Hierarchy (HI), Synchronization (SY), and Characteristic path length (CPL). In addition, the 360 features of each local measures in the binary network are also calculated, including the clustering coefficient (CC), local efficiency (LC), betweenness centrality (BC), eigenvector centrality (EC), degree (D), and shortest path (SP). For each subject, the features are combined to form the final feature vector comprised of 2,166 measures (6×1 global measures and 6×360 local measures). All the measures are standardized to $[-1, 1]$ prior to subsequent analysis. There measures are important for fMRI classification of Alzheimer's disease because they provide quantitative measures of structural and functional changes in AD brain network. The differences in measures between AD and HC involve disruptions in connectivity between brain regions, inefficient information transmission, and changes in central nodes.

B. FEATURE SELECTION

Network-based measures generated candidate features for classification. These features could be noisy and irrelevant, leading to overfitting issues and calculation cost and classification accuracy. A feature selection algorithm is an important part of machine learning, which helps to strengthen the understanding between features and eigenvalues, reduce the number of features, and improve classification accuracy. In the feature selection section, three feature selection algorithms are applied to classification (Figure 1).

1) MINIMAL REDUNDANCY MAXIMAL RELEVANCE SELECTION ALGORITHM (MRMR)

As part of the feature selection process, we use the MRMR algorithm, which is primarily used to identify the best m features by maximizing the correlation between features and target variables. MRMR [42] is defined as follows:

$$MRMR = \mathrm{MAX}_s \left\{ \frac{1}{|S|} \sum\nolimits_{x_i \in s} I(x_i; c) - \frac{1}{|S|^2} \sum\nolimits_{x_i, x_j \in s} I(x_i, x_j) \right\} \tag{3}$$

The correlation between the features set S and the class C is defined by the average value of all mutual information values between each feature x_i and C. Finally, we demand the feature set S with the maximum correlation-minimum redundancy.

2) SPARSE LINEAR REGRESSION FEATURE SELECTION ALGORITHMS BASED ON STATIONARY SELECTION (SS-LR)

The linear regression model [10] is defined as:

$$f(X) = Xw \tag{4}$$

where the coefficient of the linear regression is defined as $w = (w_1, w_2, \cdots, w_n)$, $f(X)$ is the predicted label vector obtained by distinguishing unknown samples. Let $L(w)$ be the loss function of linear regression to control the complexity of the model with the regularization term, which is defined as:

$$L(w) = \min_w \frac{1}{n} \|f(X) - Y\|_2^2 + \lambda \|w\|_1 \tag{5}$$

where $\lambda > 0$ is the regularization parameter of the model control.

3) FISHER SCORE FEATURE SELECTION ALGORITHMS

The within-class distance is as small as possible and the between-class distance is as high as possible, according to the Fisher score (FS) [43], a trait with good discriminative performance. The Fisher score for each feature in two class problems is computed as follows:

$$F(Z) = tr\left\{ \left(\widetilde{S_b}\right) \left(\widetilde{S_w} + \gamma I\right)^{-1} \right\} \tag{6}$$

where γ is a positive regularization parameter, $\widetilde{S_b}$ is called a between-class scatter matrix, and $\widetilde{S_w}$ is called a within-class scatter matrix.

C. CLASSIFICATION

After feature selection, the top 30 features identified by three feature selection algorithms are used with the SVM classifier to find an optimal classification accuracy. The LIBSVM toolbox (http://www.csie.ntu.edu.tw/cjlin/libsvm/) is used in this paper to apply an SVM-linear algorithm to classification in MATLAB. The SVM-linear is defined as follows:

$$\min_{w,b} \left[\frac{\|w\|^2}{2} + C \sum\nolimits_{i=1}^{N} \xi_i \right], \quad y_i (w \cdot x_i + b) \geq 1 - \xi_i, \quad \forall (x_i, y_i) \in D(\xi_i \geq 0) \tag{7}$$

where x_1 and x_2 are two eigenvectors and C is an optimal value for the penalized coefficient. The constrained problem of maximizing the soft interval is transformed into an unconstrained problem by the Lagrange function:

$$L(w, b, \xi, \alpha, \mu) = \frac{\|w\|^2}{2} + C \sum\nolimits_{i=1}^{N} \xi_i - \sum\nolimits_{i=1}^{m} \alpha_i \left[y_i \left(w^T x_i + b \right) - 1 + \xi_i \right] - \sum\nolimits_{i=1}^{m} \mu_i \xi_i \tag{8}$$

Then, we use SVM-linear and the optimal subsets for classification of difference stages of cognitive impairment (EMCI, LMCI and AD) and normal group. The K-fold (k = 5) class-validation (KCV) approach is employed to evaluate performance of SVM-linear. In each fold of KCV, 80% of the data are selected for training the model, while the remaining 20% are selected for calculating accuracy by using SVM.

D. NETWORK-BASED STATISTIC (NBS) ANALYSIS

To identify the specific altered functional connectivity [44] pattern in AD, the network-based statistic (NBS) [45]

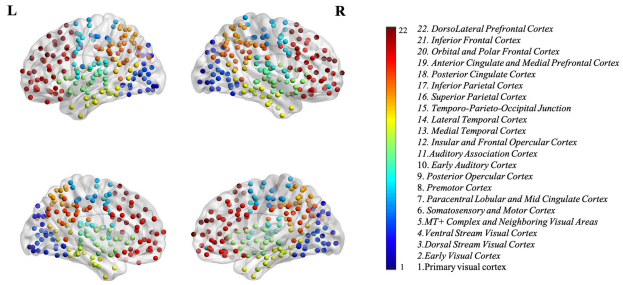

FIGURE 3. Nodes of the graph defined by 360 functional areas into 22 regions. Each region in different colours is displayed on lateral and medial views of the left and right hemisphere inflated cortical surfaces. Figures are all generated by MATLAB toolbox with BrainNet Viewer 2019 software package (www.nitrc.org/projects/bnv/).

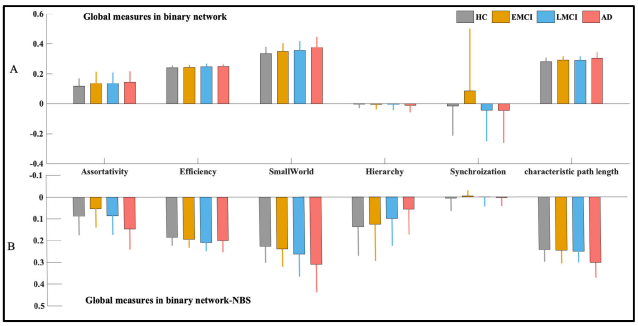

FIGURE 5. Six global measures in the binary network and global measures in the binary network after NBS between the four groups (HC, EMCI, LMCI and AD). Figures are all generated by MATLAB toolbox with GRETNA software package.

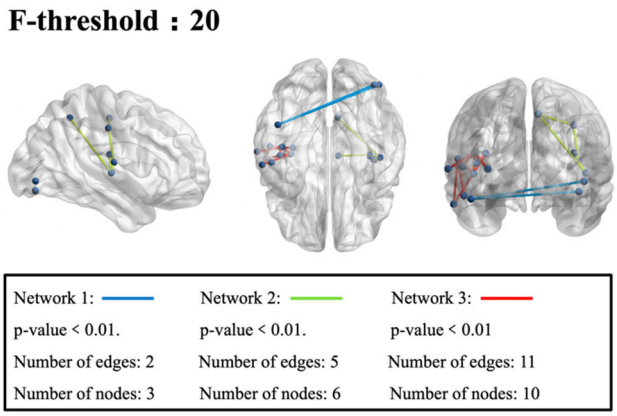

FIGURE 4. Significant differences in the interregional connections (edges) among the four groups (HC, EMCL, LMCI, AD) at an F-threshold of 20. The statistical analysis using the NBS method identifies three significantly altered networks at an F-threshold of 20. Figures are all generated by MATLAB toolbox with BrainNet Viewer 2019 software package (www.nitrc.org/projects/bnv/).

(https://www.nitrc.org/projects/nbs/) approach is utilized. This approach is a nonparametric method, which can control the familywise error rate when calculating multiple test statistics to evaluate network connectivity. An F-threshold analysis is performed in the NBS analysis method to determine the functional networks that differ among the four groups. Then, the subjects are randomly assigned to a group to perform the permutation testing (n = 10000) to find the empirical null distribution of the largest connected component size. A range of primary threshold values (F-threshold) is examined from 10 to 30 by a step of 1.

V. RESULTS

A. GLOBAL AND LOCAL STATISTICAL ANALYSIS OF GRAPH MEASURES

By analyzing the connectivity matrices of all subjects, we conduct NBS analysis with 10,000 random permutations to determine if there are any disrupted patterns of connectivity for the largest connected component. At a high F-threshold, there is no significant network, but at a low F-threshold, there are significant networks with many connections. Three networks of 2, 5 and 11 are found to have disturbed functional connectivity patterns in the four groups when NBS is applied on the raw connectivity with the F-threshold of 20 ($p < 0.001$, corrected for multiple comparisons) in Figure 4. The first network comprises two edges (i.e., connections) and three nodes (i.e., brain areas) with Right Area 55b (R_55b), Right Posterior InferoTemporal (R_PIT), and Left Area TF (L_TF). The second network comprises five edges and six nodes with Right Primary Auditory Cortex (R_A1), Right Area 6m anterior (R_6ma), Right Area 3a (R_3a), Right Area 10d (R_10d), Right Area posterior 10p (R_p10p), and Right Area STSv anterior (R_STSva). The third network comprises eleven edges and ten nodes with Left Area 3a (L_3a), Left Area 45 (L_45), Left Area IFSa (L_IFsa), Left Area anterior 9-46v (L_a9-46v), Left Area 52 (L_52), Left ProStriate Area (L_ProS), Left Area TE1 posterior (L_TE1p), Left Medial Belt Complex (L_MBelt), Left Auditory 4 Complex (L_A4), and Left Area STSv anterior (L_STSva). As a result, the results remain unchanged when using the false discovery rate (FDR) method with 10,000 permutations.

The NBS analysis is performed to identify disrupted connectivity patterns in patients with AD, EMCI, LMCI and HC, and there are found the significant networks of 19 nodes, including R_55b, R_PIT, R_A1, R-6ma, R_3a, R_10d, R_p10p, R_STSva, L_3a, L_45,L_TFSa, L_a9-46v, L_52, L-ProS, L_TE1p, L_TF, L_MBelt, L_A4, and L_STSva. Thus, the 19×19 connectivity matrix is generated as binary network-NBS, with 19 being the number of areas included in the significant network for each participant. The six global measures with ASS, Globe GE, SW, HI, SY, and CPL in the binary network of the 360×360 connectivity matrix and binary network-NBS of the 19×19 connectivity matrix are shown in Figure 5. For D, BC, LC, CC, EC, and SP, there are no significant differences in the six globe measures with binary network and binary network-NBS based on local measures of binary networks.

Each local measure has 360 values for each subject, and each subject has a total of 2160 local values (360×6). The 61 local values with a P value < 0.01 for significant differences among the four groups (i.e., HC, EMCI, LMCI

TABLE 2. The 36 brain areas of 360 brain areas have local measures that are significantly different among the four groups (HC, EMCI, LMCI and AD). The right six columns correspond to local measures. The numbers in these columns represent a p-value < 0.01 in the four groups of corresponding areas.

Areas	22 regions	EC	LC	D	CC	SP	BC
R_V8	the ventral stream visual cortex	0.0032	—	0.0078	—	—	—
R_55b	the premotor cortex	0.0029	0.0077	0.0027	0.0096	—	—
R_A1	early auditory cortex	—	0.0021	—	0.0005	—	—
R_6ma	the sensori-motor associated paracentral lobular and mid cingulate cortex	0.0009	—	0.0021	—	0.0011	—
R_3a	somatosensory and motor cortex	0.0043	—	—	—	0.0071	—
R_6mp	the sensori-motor associated paracentral lobular and mid cingulate cortex	—	—	—	—	—	0.0034
R_8Av	the dorsolateral prefrontal cortex	0.0039	—	—	—	0.0099	—
R_9m	anterior cingulate and medial prefrontal cortex	0.0071	—	—	—		—
R_8BL	the dorsolateral prefrontal cortex	0.0033	—	—	—	0.0017	0.0092
R_10d	orbital and polar frontal cortex	0.0071	0.0011	0.0001	0.0076	—	—
R_8C	the dorsolateral prefrontal cortex	—	—	—	—	—	0.0015
R_44	inferior frontal cortex	—	—	—	0.0063	—	—
R_a47r	orbital and polar frontal cortex	0.0006	—	—	—	—	—
R_PBelt	early auditory cortex	—	0.0050	—	0.0001	—	0.0007
R_PHA3	medial the temporal cortex	—	—	0.0073	—	—	—
R_STSvp	association auditory cortex	—	—	—	0.0044	—	—
R_TE1p	lateral temporal cortex	—	—	—	0.0056	—	—
R_p10p	orbital and polar frontal cortex	0.0083	—	—	—	—	—
R_STSva	association auditory cortex	—	—	—	—	—	0.0016
L_V3	early visual cortex	—	0.0076	—	0.0075	—	—
L_3b	somatosensory and motor cortex	—	—	—	—	—	0.0078
L_3a	somatosensory and motor cortex	—	0.0062	—	0.0090	—	—
L_9m	anterior cingulate and medial prefrontal cortex	0.0034	—	—	—	0.0069	—
L_10d	orbital and polar frontal cortex	0.0002	0.0016	0.0028	—	—	—
L_45	inferior frontal cortex	—	0.0081	—	—	—	—
L_IFSa	inferior frontal cortex	—	0.0053	—	0.0035	—	—
L_a9-46v	the dorsolateral prefrontal cortex	0.0078	—	—	—	0.0052	—
L_9-46d	the dorsolateral prefrontal cortex	0.0080	—	—	—	—	—
L_47s	orbital and polar frontal cortex	—	—	0.0035	—	—	—
L_ProS	the posterior cingulate cortex	0.0096	—	—	—	—	—
L_STSda	association auditory cortex	—	—	0.0069	—	—	—
L_STSvp	association auditory cortex	—	0.0058	—	—	0.0034	—
L_TE1p	lateral temporal cortex	—	—	—	0.0085	—	—
L_TE2a	lateral temporal cortex	—	—	0.0070	—	—	0.0030
L_TF	lateral temporal cortex	—	—	—	—	—	0.0021
L_lg	the insular and frontal opercular cortex	—	0.0089	—	—	—	—

Note: Nodal degree (D), betweenness centrality (BC), local efficiency (LC), clustering coefficient (CC), eigenvector centrality (EC) and shortest path (SP). "—" represents p-value>0.01

and AD) are selected from 2160 local values. According to Table 1, 61 values of significantly different local measures are shown for the 22 regions of the multimodal cortical parcellation, which correspond to the 36 brain areas. With reference to the 22 regions in Fig.3, these 36 brain areas are mainly located in the early visual cortex (RGN 2; Left Third Visual Area (L_V3)), ventral stream visual cortex (RGN 4; Right Eighth Visual Area (R_V8)), somatosensory and motor cortex (RGN 6; R_3a, Left Primary Sensory Cortex (L_3b), and L_3a), sensorimotor-associated paracentral lobular and mid cingulate cortex (RGN 7; R_6ma and Right Area 6mp (R_6mp)), premotor cortex (RGN 8; R_55b), early auditory cortex (RGN 10; R_A1 and Right ParaBelt Complex (R_PBelt)), association auditory cortex (RGN 11; R_STSva, Right Area STSv posterior (R_STSvp), Left Area STSd anterior (L_STSda), and Left Area STSv posterior (L_STSvp)), insular and frontal opercular cortex (RGN 12; Left Insular Granular Complex (L_lg)), medial temporal cortex (RGN 13; Right ParaHippocampal Area 3 (R_PHA3)), lateral temporal cortex (RGN 14; Left Area TE1 posterior (R_TE1p), L_TE1p, Left TE2 anterior (L_TE2a), and L_TF), posterior cingulate cortex (RGN 18; L_ProS), anterior cingulate and medial prefrontal cortex (RGN 19; Right Area 9 Middle (R_9m) and Left Area 9 Middle (L_9m)), orbital and polar frontal cortex (RGN 20; R_10d, R_p10p, Left Area 10d (L_10d), and Left Area 47s (L_47s)), inferior frontal cortex (RGN 21; Right Area 44 (R_44), Left Area 45 (L_45), Left Area IFSa (L_IFSa), and Right Area anterior 47r (R_a47r)), and dorsolateral prefrontal cortex (RGN 22; Right Area 8Av (R_8Av), Right Area 8B Lateral (R_8BL), Right Area 8C (R_8C), Left Area anterior 9-46v (L_a9-46v), and Left Area 9-46d (L_9-46d)), as shown in Table 2. As a result, most of these brain areas are located within one of the six multimodal cortical parcellation regions (somatosensory and motor cortex (RGN 6), association auditory cortex (RGN 11), lateral temporal cortex (RGN 14), orbital and polar frontal

cortex (RGN 20), inferior frontal cortex (RGN 21) and dorsolateral prefrontal cortex (RGN 22)) with more than three areas. The following 14 brain areas are found to be identical between the 19 brain areas extracted by NBS analysis and the 36 brain areas: R_55b, R_A1, R-6ma, R_3a, R_10d, R_p10p, R_STSva, L_3a, L_45, L_TFSa, L_a9-46v, L-ProS, L_TE1p, and L_TF.

B. CLASSIFICATION RESULTS USING GLOBAL AND LOCAL MEASURES

As we all know, using a high-dimensional feature space for classification is time-consuming, and the classification performance is poor due to the existence of redundant and irrelevant features. We classify the HC vs. EMCI, HC vs. LMCI, HC vs. AD, EMCI vs. LMCI, LMCI vs. AD, and EMCI vs. AD in four different situations, including 360 areas using local graph measures, 360 areas using local graph measures plus global graph measures, 36 areas using local graph measures again, and 360 areas using global graph measures. Thus, the corresponding feature vector sizes are 2,160 ($6 \times 360 = 2{,}160$ local features), 2,166 (6×360 local features + 6 global features = 2166), 216 ($6 \times 36 = 216$ local features), and 6 (6 global features), respectively. After the calculation of graph measures, we utilize these features as input features of three feature selection algorithms to identify the optimal features. Feature selection algorithms are performed on the above three sets of feature vectors to select the optimal features, excluding the features of 360 areas using global graph measures.

The classification accuracy of classifiers under different feature selection algorithms is compared with significant difference. The top 30 features of the list with maximum discrimination by the MRMR algorithm are selected in a wrapper algorithm to find the optimal subset of features. 21 out of the 30 features contained information that could be associated with one of the six major brain regions: the somatosensory and motor cortex (RGN 6), association auditory cortex (RGN 11), lateral temporal cortex (RGN 14), orbital and polar frontal cortex (RGN 20), inferior frontal cortex (RGN 21), and dorsolateral prefrontal cortex (RGN 22). Then, the classification results of the 216 local features in 36 areas using three different feature selection algorithms (i.e., MRMR, SS-LR and FS) with SVM-liner are compared, as shown in Table 3. For the MRMR algorithm, the average accuracies with local measures for 36 areas achieves the best scores: 85.60%, 92.90%, 96.80%, 83.30%, 84.90% and 89.50% in terms of HC vs. EMCI, HC vs. LMCI, HC vs. AD, EMCI vs. LMCI, LMCI vs. AD, and EMCI vs. AD, respectively (Table 3). According to the quantitative results in Table 3, the MRMR algorithm achieves the best classification performance compared with the SS-LR and FS algorithms. In brief, the appropriate method may enhance the classification impact based on the classification outcomes of the three feature selection algorithms.

Subsequently, we train and test the different classifiers (SVM-linear [46], KNN, LDA, CNN, and Decision tree) using the optimal feature subset of the MRMR, and the classification accuracies corresponding to the four situations are shown in Table 4. The classification results are obtained by local measures for 36 areas with SVM-linear for distinguishing HC vs. EMCI, HC vs. LMCI, HC vs. AD, EMCI vs. LMCI, LMCI vs. AD, and EMCI vs. AD are 85.60%, 92.90%, 96.80%, 83.30%, 84.90% and 89.50%, respectively (Table 4). In short, based on the classification results of the three feature selection algorithms, the right approach may improve the classification effect. Then, we find that the accuracies of classification are higher with 36 areas for local measures than with direct local measures calculation for 360 areas in Table 4. The classification accuracies in globe measures of 360 areas for distinguishing HC vs. EMCI, HC vs. LMCI, HC vs. AD, EMCI vs. LMCI, LMCI vs. AD, and EMCI vs. AD are 44.50%, 49.80%, 54.20%, 42.20%, 43.90% and 37.50%, respectively. The maximum classification accuracy of the globe measures is less than 58%. As shown in Table 4, we compare the results of the four classifiers using the SVM-linear, KNN, LDA, CNN and Decision tree algorithms, respectively. The classification results of the SVM-linear are better than KNN, LDA, CNN, and Decision tree in four situations. Overall, such results further demonstrate the advantage of the classification framework with dual graph measures of the MRMR and SVM-linear in the 36 local areas (Tables 3 and 4).

In particular, some previous studies have used imaging data from the ADNI dataset to assess the classification performance of different methods used to distinguish the stages of Alzheimer's disease. Table 5 shows the comparative results. It can be seen that the classification results of constructing brain function network with the multi-feature selection in different stages of AD are significantly higher accuracy than the results of other previous studies. In brief, our study provides the valuable insights into the prediction of HC $\rightarrow$ EMCI $\rightarrow$ LMCI $\rightarrow$ AD, and reveals that graph measure of fMRI is the potential predictor of classification. Consequently, this study demonstrates the usefulness of features obtained from function brain network measurements and machine learning methods based on fMRI for more accurate classification.

VI. DISCUSSION

Using the NBS analysis, we identify three fMRI networks that are significantly different in HC, EMCI, LMCI, and AD. The first network comprises two edges in three areas: R_55b, R_PIT, and L_TF. In this network, R_PIT is connected to the R_55b and L_TF. With reference to the 22 regions in Figure 3, R_PIT corresponds to the ventral stream visual cortex, which plays an essential role in DAN. Previous studies reported the existence of atrophy of visual cortices in late MCI [51]. The second network comprises five edges in six areas: R_A1, R_6ma, R_3a, R_10d, R_p10p, and R_STSva. R STSva corresponds to the auditory association cortex with reference to the 22 regions in Figure 3, which plays a crucial role in the DMN for AD [52]. Sheng et al. [1] found that 10d was one of five key brain areas, which had been confirmed

TABLE 3. Classification of results and performance of different feature selection algorithms using svm-linear for local 36 areas in the identification of four groups of HC, EMCI, LMCI and AD.

Feature selection	HC vs. EMCI	HC vs. LMCI	HC vs. AD	EMCI vs. LMCI	LMCI vs.AD	EMCI vs. AD
MRMR	**85.60%**	**92.90%**	**96.80%**	**83.30%**	**84.90%**	**89.50%**
SS-LR	83.40%	90.80%	94.90%	84.70%	84.80%	87.80%
FS	85.80%	91.20%	93.80%	80.40%	82.60%	88.80%

TABLE 4. Comparison of classification performance of different classifiers using local graph measures for 360 areas, local graph measures plus globe graph measures for 360 areas, local graph measures for 36 areas, and globe graph measures for 360 areas in the identification of four groups of HC, EMCI, LMCI and AD.

	Classifier	HC vs. EMCI	HC vs. LMCI	HC vs. AD	EMCI vs. LMCI	LMCI vs.AD	EMCI vs. AD
SVM-linear	Local 36 areas	**85.60%**	**92.90%**	**96.80%**	**83.30%**	**84.90%**	**89.50%**
	Local 360 areas	79.70%	84.40%	93.00%	77.60%	82.70%	83.80%
	Local + Globe 360 areas	77.90%	82.90%	84.70%	75.40%	77.90%	80.40%
	Globe 360 areas	44.50%	49.80%	54.20%	42.20%	43.90%	37.50%
LDA	Local 36 areas	79.40%	82.80%	90.90%	70.70%	68.80%	73.80%
	Local 360 areas	76.20%	77.30%	88.80%	69.90%	67.70%	70.70%
	Local + Globe 360 areas	74.30%	76.90%	78.90%	66.50%	68.90%	65.30%
	Globe 360 areas	44.8%	49.7%	50.8%	40.9%	40.6%	37.8%
KNN	Local 36 areas	83.40%	84.80%	88.20%	72.40%	76.80%	80.10%
	Local 360 areas	79.20%	82.30%	84.50%	72.60%	73.70%	79.70%
	Local + Globe 360 areas	69.50%	73.70%	80.90%	66.50%	65.00%	69.30%
	Globe 360 areas	40.60%	37.70%	57.80%	29.90%	32.60%	38.80%
Decision tree	Local 36 areas	74.30%	70.60%	80.80%	62.80%	66.40%	75.80%
	Local 360 areas	66.80%	69.30%	75.90%	58.90%	67.90%	72.60%
	Local + Globe 360 areas	70.80%	73.80%	72.40%	47.90%	64.70%	70.90%
	Globe 360 areas	40.8%	48.2%	40.8%	30.4%	39.6%	33.8%
CNN	Local 36 areas	82.7%	91.0%	95.5%	82.1%	85.0%	87.6%
	Local 360 areas	80.2%	84.2%	91.8%	77.2%	83.2%	81.9%
	Local + Globe 360 areas	75.8%	80.9%	85.7%	76.8%	70.5%	80.1%
	Globe 360 areas	34.9%	56.8%	52.4%	39.0%	40.4%	42.7%

TABLE 5. Classification performance of different methods to distinguish different stages of AD.

Authors	Target	Modality	Method	Brain Segmentation Method	Accuracy (%)
Alorf et al.[47]	HC vs. LMCI	fMRI	SSAE	AAL	87.81
	HC vs. EMCI				86.79
	HC vs. AD				94.17
Basaia et al.[48]	HC vs. AD	sMRI	CNN	GM, VM, CSF	98.2
	HC vs. MCIc				87.7
	HC vs. MCIs				76.4
	AD vs MCIc				75.8
	MCIs vs. AD				86.3
	MCIc vs MCIs				74.9
Zhang et al.[10]	MCIc vs. MCInc	Rs-fMRI + sMRI	Graph theory + RSFS + SVM	AAL	84.71
	MCIc vs. AD				89.80
Duc et al.[49]	HC vs. AD	fMRI	SVM-REF + 3D-CNN	AAL	85.27
Li et al.[50]	AD vs. HC	MRI+PET	Multi-task deep learning with dropout + SVM	93 volumetric regions	91.40
	MCI vs. HC				77.40
	AD vs. MCI				70.10
	MCIc. vs. MCInc				57.40
Our Method	HC vs. EMCI	fMRI	Graph theory + MRMR + Linear-SVM	J-HCPMMP (36 areas)	**85.60**
	HC vs. LMCI				**92.90**
	HC vs. AD				**96.80**
	EMCI vs. LMCI				**83.30**
	LMCI vs.AD				**84.90**
	EMCI vs. AD				**89.50**

Note: "MCIc" means MCI-converted, "MCInc" means MCI-non converted, "MCIs" means MCI-stable

to be involved in AD. The third network comprises eleven edges in ten areas: L_3a, L_45, L_IFsa, L_a9-46v, L_52, L_ProS, L_TE1p, L_MBelt, L_A4, and L_STSva. The Our finding for association of L_a9-46v to AD is in agreement with previous studies [53] reporting. The maximum power in the left a9-46v shows high performance of AD-MCI and cognitively unimpaired participants classification. Consistent with our findings, previous studies [53], [54] demonstrated an association of ProS, STSva, A4, MBelt, and a9-46v to AD.

As listed in Table 2, the brain network properties of the four groups are compared using local measures. These 36 areas are corresponded to the 14 regions of multimodal cortical parcellation regions. However, there are more than three areas in each of the six main regions of the multimodal cortical parcellation region. Dorsolateral prefrontal cortex (R_8Av, R_8BL, R_8C, L_a9-46v, and L_9-46d), orbital and polar frontal cortex (R_10d, R_p10p, L_10d, and L_47s), and association auditory cortex (R_STSva, R_STSvp, L_STSda, and

L_STSvp) are part of DMN and DAN. It agrees with previous [7], [52], [55], [56] studies that alterations of DMN and DAN take an important role during the process in different stages of AD. It is noteworthy that 36 areas are selected from 360 areas by calculating local measures. The 21 features of the 30 optimal features selected using MRMR algorithm are related to the six main regions with RGN 6, RGN 11, RGN 14, RGN 20, RGN 21, and RGN 22. The six primary brain areas match the six primary regions that are previously mentioned. These findings are in line with other research [57], [58] that indicates these brain areas play a significant role in the progression of AD. Duc et al. [49] revealed that the medial visual, default mode, right dorsal attention, executive, salience, auditory related, cerebellar, left dorsal attention, and frontal networks statistically differed between AD and HC conditions. Albers et al. [59] that the sensory and motor areas of the central nervous system were obviously affected by AD pathology, and the intervention measures aimed at improving AD sensorimotor defects might enhance the patient's function with the progress of AD. The auditory association cortex is activated in the LANGUAGE STORY, MATH, and STOEY-MATH contrasts [35]. As compared to patients with greater cognitive function, Alana et al. [60] reported that individuals with mini-mental state examination (MMSE) $\leq$ 25 and AD had lower grey matter density in the association auditory cortex. Buchanan et al. [61] revealed that synaptic loss, endoplasmic reticulum stress and neuro-Inflammation emerged late in the lateral temporal cortex, and selectively correlated with cognitive decline in Alzheimer's disease. Yao et al. [62] found interregional correlation changes were detected in the para hippocampus gyrus, medial temporal lobe, cingulum, fusiform, medial frontal lobe, and orbital frontal gyrus in groups with MCI and AD. Dekosky et al. [63] found that cortical and hippocampal choline acetyltransferase activity in the superior frontal cortex were significantly elevated above normal controls in MCI subjects. Kumar et al. [64] suggested that the dorsolateral prefrontal cortex plasticity was significant deficits in Alzheimer's patients, compared with controls. Joseph et al. [65] revealed that Alzheimer's patients had increased dorsolateral prefrontal cortex excitability, which was negatively correlated with overall cognitive and executive function. Our findings are consistent with those associated with selected brain regions that have previously been shown to be associated with AD. These regions are among the earliest to show abnormal amyloid deposition, which play an important role in EMCI, LMCI and AD.

In this study, we use the fMRI and dual graph theory with the multi-feature selection method to accurately classify patients. In the classification of HC vs. EMCI, HC vs. LMCI, HC vs. AD, EMCI vs. LMCI, LMCI vs. AD, and EMCI vs. AD, compared with other algorithms, MRMR algorithm and SVM-liner with based on local measures for 36 areas achieve the best accuracies (Table 3 and 4), which demonstrates that the high-level topological information of the brain connectivity selected by multi-feature algorithm is useful for classifying Alzheimer's disease. Table 4 illustrates that only local measures for 36 areas produce the highest classification accuracy (local measures for 36 areas > local measures for 360 areas > local measures plus globe measures for 360 areas > only globe measures for 360 areas). As a result of our analysis, it is evident that local measures in the functional network contain more disease information, and the top 30 selected features are more sensitive to efficient classification. Furthermore, some local graph measures are significantly different within certain brain regions, such as medial temporal lobe region, occipital region, precuneus region, sensory/somatomotor region, and visual region. It suggests that selecting the appropriate feature selection algorithm and local measures can improve the classification accuracy of the difference stages of AD. Ultimately, local network measures can effectively select key brain areas, greatly expand our understanding of AD classification, and provide clues to new potential diagnostic markers (highly sensitive features) located in brain areas.

The maximum classification accuracy of the global measures is lower than 58%, which shows that there are no noteworthy variations in the global measurements for the HC, EMCI, LMCI, and AD groups, it is consistent with the results in Figure 5. Some studies [34], [66], [67] have shown that the functional changes of cognitive impairment in the whole brain are weaker than those in local brain areas. It has been reported there were no significant difference in values of global efficiency [68] and clustering coefficient [68], [69] between HC and AD groups. Khazaee et al. [30] did not find any significant differences among HC, MCI, and AD groups in global measures, including clustering coefficient, characteristic path length, global efficiency, and assortativity.

Thus, binary networks are constructed for four groups based on fMRI and J-HCPMMP parcellation. The main 36 areas are derived from 360 areas by using local measures. The use of multi-feature extraction method can obtain more accurate classification and better reflect the functional changes of cognitive impairment in local brain areas. 36 diseases' extremely sensitive areas are chosen as they help with categorization more effectively. In addition, cognitive impairment fails to respond effectively to global measures. In short, our study provides the valuable insights into the prediction of HC $\rightarrow$ EMCI $\rightarrow$ LMCI $\rightarrow$ AD, graph theory and multi-feature selection algorithm are used to study brain network, discover the differences caused by AD. Consequently, this study demonstrated the usefulness of features obtained from function brain network measurements and machine learning methods based on fMRI for more accurate classification.

Here are some possible directions for future work in relation to the classification of functional brain network in Alzheimer's disease. Firstly, we can expand the sample size to include more patients and healthy control groups to more accurately capture the impact of Alzheimer's disease on the brain network. Additionally, longitudinal study designs can

be adopted to track changes in brain network metrics as the disease progresses, providing insights into their relationship with disease development. Secondly, we can explore methods for multimodal data (i.e., sMRI data, genetic data, biomarkers or clinical data) fusion and evaluate their effectiveness in Alzheimer's disease classification. Thirdly, to confirm the reliability and consistency of the classification model, future work can conduct validation and replication studies on multiple independent datasets. This helps determine the applicability of the model to different datasets and different populations. There are some potential directions for future work on the classification of Alzheimer's disease with fMRI, helping to future advance research in this field and facilitate the development of clinical applications.

VII. CONCLUSION

In summary, we develop and evaluate the multi-feature selection model using graph measures and machine learning to identify optimal features for classifying HC, EMCI, LMCI and AD. Specifically, we first employ J-HCPMMP brain parcellation approach to construct brain functional connectivity network for each subject. Then, the multi-feature selection model with dual graph measures is designed to identify optimal features. Thirty features are selected to achieve the optimal classification accuracies of 85.6% for HC vs. EMCI, 92.9% for HC vs. LMCI, 96.8% for HC vs. AD, 83.3% for EMCI vs. LMCI, 84.9% for LMCI vs. AD, and 89.5% for EMCI vs. AD respectively by using MRMR algorithm and SVM based local measures. By comparing the classification results, we find that the selected local measures show more effective features derived from the functional brain network than the global measures. Informative graph measures are related to the brain cortical regions and provided information about disrupted brain functional regions. In light of this, our results show that cognitive impairment based on functional connectivity networks with graph measures may enhance the classification accuracy of the various phases of AD.

REFERENCES

[1] J. Sheng, M. Shao, Q. Zhang, R. Zhou, L. Wang, and Y. Xin, "Alzheimer's disease, mild cognitive impairment, and normal aging distinguished by multi-modal parcellation and machine learning," *Sci. Rep.*, vol. 10, no. 1, p. 5475, Mar. 2020.

[2] O. V. Billette, "Novelty-related fMRI responses of precuneus and medial temporal regions in individuals at risk for Alzheimer disease," *Neurology*, vol. 99, no. 8, pp. e775–e788, Aug. 2022.

[3] M. Ewers, Y. Luan, L. Frontzkowski, and J. Neitzel, "Segregation of functional networks is associated with cognitive resilience in Alzheimer's disease," *Brain*, vol. 144, no. 7, pp. 2176–2185, Jul. 2021.

[4] L. Passamonti, K. A. Tsvetanov, P. S. Jones, W. R. Bevan-Jones, R. Arnold, R. J. Borchert, E. Mak, L. Su, J. T. O'Brien, and J. B. Rowe, "Neuroinflammation and functional connectivity in Alzheimer's disease: Interactive influences on cognitive performance," *J. Neurosci.*, vol. 39, no. 36, pp. 7218–7226, Sep. 2019.

[5] F. V. Farahani, W. Karwowski, and N. R. Lighthall, "Application of graph theory for identifying connectivity patterns in human brain networks: A systematic review," *Frontiers Neurosci.*, vol. 13, p. 585, Jun. 2019.

[6] F. Vecchio, F. Miraglia, and P. M. Rossini, "Connectome: Graph theory application in functional brain network architecture," *Clin. Neurophysiol. Pract.*, vol. 2, pp. 206–213, Oct. 2017.

[7] P.-J. Toussaint, S. Maiz, D. Coynel, J. Doyon, A. Messé, L. C. de Souza, M. Sarazin, V. Perlbarg, M.-O. Habert, and H. Benali, "Characteristics of the default mode functional connectivity in normal ageing and Alzheimer's disease using resting state fMRI with a combined approach of entropy-based and graph theoretical measurements," *NeuroImage*, vol. 101, pp. 778–786, Nov. 2014.

[8] U. Khatri and G.-R. Kwon, "Alzheimer's disease diagnosis and biomarker analysis using resting-state functional MRI functional brain network with multi-measures features and hippocampal subfield and amygdala volume of structural MRI," *Frontiers Aging Neurosci.*, vol. 14, May 2022, Art. no. 818871.

[9] Q. Behfar, S. K. Behfar, B. von Reutern, N. Richter, J. Dronse, R. Fassbender, G. R. Fink, and O. A. Onur, "Graph theory analysis reveals resting-state compensatory mechanisms in healthy aging and prodromal Alzheimer's disease," *Frontiers Aging Neurosci.*, vol. 12, Oct. 2020, Art. no. 576627.

[10] T. Zhang, Q. Liao, D. Zhang, C. Zhang, J. Yan, R. Ngetich, J. Zhang, Z. Jin, and L. Li, "Predicting MCI to AD conversation using integrated sMRI and rs-fMRI: Machine learning and graph theory approach," *Frontiers Aging Neurosci.*, vol. 13, p. 429, Jul. 2021.

[11] S. H. Hojjati, A. Ebrahimzadeh, A. Khazaee, and A. Babajani-Feremi, "Predicting conversion from MCI to AD using resting-state fMRI, graph theoretical approach and SVM," *J. Neurosci. Methods*, vol. 282, pp. 69–80, Apr. 2017.

[12] P. R. Raamana, M. W. Weiner, L. Wang, and M. F. Beg, "Thickness network features for prognostic applications in dementia," *Neurobiol. Aging*, vol. 36, pp. S91–S102, Jan. 2015.

[13] J. Zamani, A. Sadr, and A. H. Javadi, "Classification of early-MCI patients from healthy controls using evolutionary optimization of graph measures of resting-state fMRI, for the Alzheimer's disease neuroimaging initiative," *PLoS ONE*, vol. 17, no. 6, Jun. 2022, Art. no. e0267608.

[14] S. H. Hojjati, A. Ebrahimzadeh, and A. Babajani-Feremi, "Identification of the early stage of Alzheimer's disease using structural MRI and resting-state fMRI," *Frontiers Neurol.*, vol. 10, p. 904, Aug. 2019.

[15] W. Li, X. Lin, and X. Chen, "Detecting Alzheimer's disease based on 4D fMRI: An exploration under deep learning framework," *Neurocomputing*, vol. 388, pp. 280–287, May 2020.

[16] R. Jing, "Altered large-scale dynamic connectivity patterns in Alzheimer's disease and mild cognitive impairment patients: A machine learning study," *Hum. Brain Mapping*, vol. 44, no. 9, pp. 3467–3480, Mar. 2023.

[17] J. Cruzat, R. Herzog, P. Prado, Y. Sanz-Perl, R. Gonzalez-Gomez, S. Moguilner, M. L. Kringelbach, G. Deco, E. Tagliazucchi, and A. Ibañez, "Temporal irreversibility of large-scale brain dynamics in Alzheimer's disease," *J. Neurosci.*, vol. 43, no. 9, pp. 1643–1656, Mar. 2023.

[18] H. Zhang, R. Song, L. Wang, L. Zhang, D. Wang, C. Wang, and W. Zhang, "Classification of brain disorders in rs-fMRI via local-to-global graph neural networks," *IEEE Trans. Med. Imag.*, vol. 42, no. 2, pp. 444–455, Feb. 2023.

[19] D. Yao, J. Sui, M. Wang, E. Yang, Y. Jiaerken, N. Luo, P.-T. Yap, M. Liu, and D. Shen, "A mutual multi-scale triplet graph convolutional network for classification of brain disorders using functional or structural connectivity," *IEEE Trans. Med. Imag.*, vol. 40, no. 4, pp. 1279–1289, Apr. 2021.

[20] J. Sui, R. Jiang, J. Bustillo, and V. Calhoun, "Neuroimaging-based individualized prediction of cognition and behavior for mental disorders and health: Methods and promises," *Biol. Psychiatry*, vol. 88, no. 11, pp. 818–828, Dec. 2020.

[21] H. Ahmadi, E. Fatemizadeh, and A. Nasrabadi, "Investigation of nonlinear functional connectivity in Alzheimer's disease utilizing resting state fMRI data and graph theory," *Iran. J. Biomed. Eng.*, vol. 14, no. 3, pp. 235–249, Oct. 2020.

[22] N. Chauhan and B.-J. Choi, "Comparison of functional connectivity analysis methods in Alzheimer's disease," *Appl. Sci.*, vol. 12, no. 16, p. 8096, Aug. 2022.

[23] J. DelEtoile and H. Adeli, "Graph theory and brain connectivity in Alzheimer's disease," *Neuroscientist*, vol. 23, no. 6, pp. 616–626, 2017.

[24] Z. Dai, C. Yan, K. Li, Z. Wang, J. Wang, M. Cao, Q. Lin, N. Shu, M. Xia, Y. Bi, and Y. He, "Identifying and mapping connectivity patterns of brain network hubs in Alzheimer's disease," *Cerebral Cortex*, vol. 25, no. 10, pp. 3723–3742, Oct. 2015.

[25] Z. Gao, Y. Feng, C. Ma, K. Ma, Q. Cai, and a. for the Alzheimer's Disease Neuroimaging Initiative, "Disrupted time-dependent and functional connectivity brain network in Alzheimer's disease: A resting-state fMRI study based on visibility graph," *Current Alzheimer Res.*, vol. 17, no. 1, pp. 69–79, Mar. 2020.

[26] P. Wang, B. Zhou, H. Yao, Y. Zhan, Z. Zhang, Y. Cui, K. Xu, J. Ma, L. Wang, N. An, X. Zhang, Y. Liu, and T. Jiang, "Aberrant intra- and inter-network connectivity architectures in Alzheimer's disease and mild cognitive impairment," *Sci. Rep.*, vol. 5, no. 1, pp. 1–12, Oct. 2015.

[27] S. Golbabaei, A. Dadashi, and H. Soltanian-Zadeh, "Measures of the brain functional network that correlate with Alzheimer's neuropsychological test scores: An fMRI and graph analysis study," in *Proc. 38th Annu. Int. Conf. IEEE Eng. Med. Biol. Soc. (EMBC)*, Aug. 2016, pp. 5554–5557.

[28] G. Uysal and M. Ozturk, "Classifying early and late mild cognitive impairment stages of Alzheimer's disease by analyzing different brain areas," in *Proc. Med. Technol. Congr. (TIPTEKNO)*, Nov. 2020, pp. 1–4.

[29] Y. Luo, T. Sun, C. Ma, X. Zhang, Y. Ji, X. Fu, and H. Ni, "Alterations of brain networks in Alzheimer's disease and mild cognitive impairment: A resting state fMRI study based on a population-specific brain template," *Neuroscience*, vol. 452, pp. 192–207, Jan. 2021.

[30] A. Khazaee, A. Ebrahimzadeh, and A. Babajani-Feremi, "Application of advanced machine learning methods on resting-state fMRI network for identification of mild cognitive impairment and Alzheimer's disease," *Brain Imag. Behav.*, vol. 10, no. 3, pp. 799–817, Sep. 2016.

[31] S. H. Hojjati, A. Ebrahimzadeh, A. Khazaee, and A. Babajani-Feremi, "Predicting conversion from MCI to AD by integrating rs-fMRI and structural MRI," *Comput. Biol. Med.*, vol. 102, pp. 30–39, Nov. 2018.

[32] R. K. Lama and G. R. Kwon, "Diagnosis of Alzheimer's disease using brain network," *Frontiers Neurosci.*, vol. 15, Feb. 2021, Art. no. 605115.

[33] T. Zhang, Z. Zhao, C. Zhang, J. Zhang, Z. Jin, and L. Li, "Classification of early and late mild cognitive impairment using functional brain network of resting-state fMRI," *Frontiers Psychiatry*, vol. 10, p. 572, Aug. 2019.

[34] J. Sheng, B. Wang, Q. Zhang, Q. Liu, Y. Ma, W. Liu, M. Shao, and B. Chen, "A novel joint HCPMMP method for automatically classifying Alzheimer's and different stage MCI patients," *Behavioural Brain Res.*, vol. 365, pp. 210–221, Jun. 2019.

[35] M. F. Glasser, T. S. Coalson, E. C. Robinson, C. D. Hacker, J. Harwell, E. Yacoub, K. Ugurbil, J. Andersson, C. F. Beckmann, M. Jenkinson, S. M. Smith, and D. C. Van Essen, "A multi-modal parcellation of human cerebral cortex," *Nature*, vol. 536, no. 7615, pp. 171–178, Jul. 2016.

[36] V. K. Chauhan, K. Dahiya, and A. Sharma, "Problem formulations and solvers in linear SVM: A review," *Artif. Intell. Rev.*, vol. 52, no. 2, pp. 803–855, Aug. 2019.

[37] W. M. Shaban, A. H. Rabie, A. I. Saleh, and M. A. Abo-Elsoud, "A new COVID-19 patients detection strategy (CPDS) based on hybrid feature selection and enhanced KNN classifier," *Knowl.-Based Syst.*, vol. 205, Oct. 2020, Art. no. 106270.

[38] F. Li and M. Liu, "Alzheimer's disease diagnosis based on multiple cluster dense convolutional networks," *Computerized Med. Imag. Graph.*, vol. 70, pp. 101–110, Dec. 2018.

[39] S. Mishra, P. K. Mallick, H. K. Tripathy, A. K. Bhoi, and A. González-Briones, "Performance evaluation of a proposed machine learning model for chronic disease datasets using an integrated attribute evaluator and an improved decision tree classifier," *Appl. Sci.*, vol. 10, no. 22, p. 8137, Nov. 2020.

[40] H. M. Kiani, A. Shalbaf, and A. Maghsoudi, "Identification of mild cognitive impairment disease using brain functional connectivity and graph analysis in fMRI data," *Tehran Univ. Med. J.*, vol. 79, no. 2, pp. 102–111, May 2021.

[41] M. Wang, Z. Yuan, and H. Niu, "Reliability evaluation on weighted graph metrics of fNIRS brain networks," *Quant. Imag. Med. Surgery*, vol. 9, no. 5, pp. 832–841, May 2019.

[42] M. Kumar and M. R. Reddy, "A C4.5 decision tree algorithm with MRMR features selection based recommendation system for tourists," *Psychol. Educ. J.*, vol. 58, no. 1, pp. 3640–3643, Feb. 2021.

[43] K. P. M. Niyas and P. Thiyagarajan, "Feature selection using efficient fusion of Fisher score and greedy searching for Alzheimer's classification," *J. King Saud Univ. Comput. Inf. Sci.*, vol. 34, no. 8, pp. 4993–5006, Sep. 2022.

[44] J. Xue, H. Guo, Y. Gao, X. Wang, H. Cui, Z. Chen, B. Wang, and J. Xiang, "Altered directed functional connectivity of the hippocampus in mild cognitive impairment and Alzheimer's disease: A resting-state fMRI study," *Frontiers Aging Neurosci.*, vol. 11, p. 326, Dec. 2019.

[45] D. Liao, Z.-Q. Zhang, Z.-P. Guo, L.-R. Tang, M.-H. Yang, R.-P. Wang, X.-F. Liu, and C.-H. Liu, "Disrupted topological organization of functional brain networks is associated with cognitive impairment in hypertension patients: A resting-state fMRI study," *Neuroradiology*, vol. 65, no. 2, pp. 323–336, Feb. 2023.

[46] D. Madroñal, R. Lazcano, R. Salvador, H. Fabelo, S. Ortega, G. M. Callico, E. Juarez, and C. Sanz, "SVM-based real-time hyperspectral image classifier on a manycore architecture," *J. Syst. Archit.*, vol. 80, pp. 30–40, Oct. 2017.

[47] A. Alorf and M. U. G. Khan, "Multi-label classification of Alzheimer's disease stages from resting-state fMRI-based correlation connectivity data and deep learning," *Comput. Biol. Med.*, vol. 151, Dec. 2022, Art. no. 106240.

[48] S. Basaia, F. Agosta, L. Wagner, E. Canu, G. Magnani, R. Santangelo, and M. Filippi, "Automated classification of Alzheimer's disease and mild cognitive impairment using a single MRI and deep neural networks," *NeuroImage, Clin.*, vol. 21, Jan. 2019, Art. no. 101645.

[49] N. T. Duc, S. Ryu, M. N. I. Qureshi, M. Choi, K. H. Lee, and B. Lee, "3D-deep learning based automatic diagnosis of Alzheimer's disease with joint MMSE prediction using resting-state fMRI," *Neuroinformatics*, vol. 18, no. 1, pp. 71–86, Jan. 2020.

[50] F. Li, L. Tran, K.-H. Thung, S. Ji, D. Shen, and J. Li, "A robust deep model for improved classification of AD/MCI patients," *IEEE J. Biomed. Health Informat.*, vol. 19, no. 5, pp. 1610–1616, Sep. 2015.

[51] Y. Deng, L. Shi, Y. Lei, and P. Liang, "Mapping the 'what' and 'where' visual cortices their atrophy Alzheimer's disease: Combined activation likelihood estimation with voxel-based morphometry," *Front. Hum Neurosci.*, vol. 10, p. 333, Jun. 2016.

[52] D. Putcha, M. Brickhouse, D. A. Wolk, and B. C. Dickerson, "Fractionating the Rey Auditory Verbal Learning Test: Distinct roles of large-scale cortical networks in prodromal Alzheimer's disease," *Neuropsychologia*, vol. 129, pp. 83–92, Jun. 2019.

[53] M. Noguchi-Shinohara, M. Koike, H. Morise, K. Kudo, S. Tsuchimine, J. Komatsu, C. Abe, S. Kitagawa, Y. Ikeda, and M. Yamada, "MEG activity of the dorsolateral prefrontal cortex during optic flow stimulations detects mild cognitive impairment due to Alzheimer's disease," *PLoS ONE*, vol. 16, no. 11, Nov. 2021, Art. no. e0259677.

[54] M. Belghali, N. Chastan, F. Cignetti, D. Davenne, and L. M. Decker, "Loss of gait control assessed by cognitive-motor dual-tasks: Pros and cons in detecting people at risk of developing Alzheimer's and Parkinson's diseases," *GeroScience*, vol. 39, no. 3, pp. 305–329, Jun. 2017.

[55] E. Ersoezlue, "Lifelong experiences as a proxy of cognitive reserve moderate the association between connectivity and cognition in Alzheimer's disease," *Neurobiol. Aging*, vol. 122, pp. 33–44, Feb. 2023.

[56] H. Ahmadi, E. Fatemizadeh, and A. M. Nasrabadi, "A comparative study of correlation methods in functional connectivity analysis using fMRI data of Alzheimer's patients," *J. Biomed. Phys. Eng.*, vol. 13, no. 2, pp. 125–134, Apr. 2023.

[57] S. Bludau, S. B. Eickhoff, H. Mohlberg, S. Caspers, A. R. Laird, P. T. Fox, A. Schleicher, K. Zilles, and K. Amunts, "Cytoarchitecture, probability maps and functions of the human frontal pole," *NeuroImage*, vol. 93, pp. 260–275, Jun. 2014.

[58] A. M. Butts, M. M. Machulda, P. Martin, S. A. Przybelski, J. R. Duffy, J. Graff-Radford, D. S. Knopman, R. C. Petersen, C. R. Jack, V. J. Lowe, K. A. Josephs, and J. L. Whitwell, "Temporal cortical thickness and cognitive associations among typical and atypical phenotypes of Alzheimer's disease," *J. Alzheimer's Disease Rep.*, vol. 6, no. 1, pp. 479–491, Aug. 2022.

[59] M. W. Albers, "At the interface of sensory and motor dysfunctions and Alzheimer's disease," *Alzheimer's Dementia, J. Alzheimer's Assoc.*, vol. 11, no. 1, pp. 70–98, 2015.

[60] A. Aylward, P. Auduong, J. S. Anderson, B. A. Zielinski, A. Y. Wang, C. Weng, N. L. Foster, and R. K. Gurgel, "Changes in the auditory association cortex in dementing illnesses," *Otol. Neurotol.*, vol. 41, no. 10, pp. 1327–1333, Dec. 2020.

[61] H. Buchanan, M. Mackay, K. Palmer, K. Tothová, M. Katsur, B. Platt, and D. J. Koss, "Synaptic loss, ER stress and neuro-inflammation emerge late in the lateral temporal cortex and associate with progressive tau pathology in Alzheimer's disease," *Mol. Neurobiol.*, vol. 57, no. 8, pp. 3258–3272, Aug. 2020.

[62] Z. Yao, Y. Zhang, L. Lin, Y. Zhou, C. Xu, and T. Jiang, "Abnormal cortical networks in mild cognitive impairment and Alzheimer's disease," *PLoS Comput. Biol.*, vol. 6, no. 11, Nov. 2010, Art. no. e1001006.

[63] S. T. DeKosky, M. D. Ikonomovic, S. D. Styren, L. Beckett, S. Wisniewski, D. A. Bennett, E. J. Cochran, J. H. Kordower, and E. J. Mufson, "Upregulation of choline acetyltransferase activity in hippocampus and frontal cortex of elderly subjects with mild cognitive impairment," *Ann. Neurol.*, vol. 51, no. 2, pp. 145–155, Feb. 2002.

[64] S. Kumar, R. Zomorrodi, Z. Ghazala, and M. S. Goodman, "Extent of dorsolateral prefrontal cortex plasticity and its association with working memory in patients with Alzheimer disease," *JAMA psychiatry*, vol. 74, no. 12, pp. 1266–1274, Dec. 2017.

[65] S. Joseph, D. Knezevic, R. Zomorrodi, D. M. Blumberger, Z. J. Daskalakis, B. H. Mulsant, B. G. Pollock, A. Voineskos, W. Wang, T. K. Rajji, and S. Kumar, "Dorsolateral prefrontal cortex excitability abnormalities in Alzheimer's dementia: Findings from transcranial magnetic stimulation and electroencephalography study," *Int. J. Psychophysiol.*, vol. 169, pp. 55–62, Nov. 2021.

[66] S. Cai, T. Chong, Y. Peng, W. Shen, J. Li, K. M. von Deneen, and L. Huang, "Altered functional brain networks in amnestic mild cognitive impairment: A resting-state fMRI study," *Brain Imag. Behav.*, vol. 11, no. 3, pp. 619–631, Jun. 2017.

[67] S. Diciotti, S. Orsolini, E. Salvadori, A. Giorgio, N. Toschi, S. Ciulli, A. Ginestroni, A. Poggesi, N. De Stefano, L. Pantoni, D. Inzitari, and M. Mascalchi, "Resting state fMRI regional homogeneity correlates with cognition measures in subcortical vascular cognitive impairment," *J. Neurolog. Sci.*, vol. 373, pp. 1–6, Feb. 2017.

[68] E. J. Sanz-Arigita, M. M. Schoonheim, J. S. Damoiseaux, S. A. R. B. Rombouts, E. Maris, F. Barkhof, P. Scheltens, and C. J. Stam, "Loss of 'small-world' networks in Alzheimer's disease: Graph analysis of fMRI resting-state functional connectivity," *PLoS ONE*, vol. 5, no. 11, Nov. 2010, Art. no. e13788.

[69] C.-Y. Lo, P.-N. Wang, K.-H. Chou, J. Wang, Y. He, and C.-P. Lin, "Diffusion tensor tractography reveals abnormal topological organization in structural cortical networks in Alzheimer's disease," *J. Neurosci.*, vol. 30, no. 50, pp. 16876–16885, Dec. 2010.

LUYUN WANG received the B.S. degree in software engineering and the M.S. degree in computer science and technology from Hangzhou Dianzi University, Hangzhou, China, in 2015 and 2018, respectively, where she is currently pursuing the Ph.D. degree. She is also a Lecturer with the Hangzhou Vocational and Technical College, Hangzhou. Her current research interests include neuroscience and medical image processing.

JINHUA SHENG (Senior Member, IEEE) received the Ph.D. degree in nuclear electronics from the University of Science and Technology of China, in 1997.

Currently, he is a Distinguished Professor with the College of Computer Science and Technology, Hangzhou Dianzi University, the Deputy Director of Institute of "Cognitive and Intelligent Computing," Hangzhou Dianzi University, and the Director of the Key Laboratory of "Intelligent Image Analysis for Sensory and Cognitive Health," Ministry of Industry and Information Technology of China, Hangzhou, China. He has 16 years of experience at prominent universities of the United States. As a researcher and an expert in image processing, medical imaging science, machine learning, and brain and cognitive science, he has contributed a lot in his area of specialization with over 70 research papers in some peer-reviewed journals and international conferences, and he has been granted one U.S. patent, and 15 Chinese patents. He is serving as an Associate Editor for IEEE Access and an Editorial Board Member for *Scientific Reports*. He was a fellow of IET, in 2022.

QIAO ZHANG received the M.D. degree from Bengbu Medical University, China, in 1988. From May 2006 to June 2009, she was a Visiting Scholar with the Feinberg School of Medicine, Northwestern University, USA. Currently, she is a Full Professor with Beijing Hospital and Institute of Geriatric Medicine, Chinese Academy of Medical Sciences. As a researcher and a clinical expert, she has contributed a lot in clinical medicine and has published more than 40 research papers.

ROUGANG ZHOU received the B.S. degree in automation from the Harbin Institute of Technology, Harbin, China, in 2008, and the Ph.D. degree in mechanical engineering from the Huazhong University of Science and Technology.

From 2018 to 2019, he was the Chief Expert with the Institute of Intelligent Manufacturing, Haier Group. Since 2018, he has been a Professor and a Doctoral Supervisor with the School of Mechanical Engineering, Hangzhou University of Electronic Technology. His research interests include machine vision, artificial intelligence, image analysis, and intelligent manufacturing.

ZHONGJIN LI received the Ph.D. degree from the Software Institute, Nanjing University, Nanjing, China, in 2017. He is currently an Associate Professor with the College of Computer Science and Technology, Hangzhou Dianzi University, Hangzhou, China. His research interests include cloud workflow scheduling, mobile edge computing, video semantic segmentation, and machine learning.

YU XIN received the bachelor's degree in computer science and technology from the University of Jinan, China, in 2019. She is currently pursuing the Ph.D. degree with Hangzhou Dianzi University, Hangzhou, China. Her current research interests include neuroscience, imaging genomics, deep learning, and Alzheimer's disease.

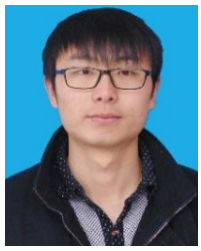

QIAN ZHANG received the master's degree from the College of Computer Science and Artificial Intelligence, Wenzhou University, China. He is currently pursuing the Ph.D. degree with the College of Computer Science, Hangzhou Dianzi University, China. His research interests include evolutionary computation, meta-heuristic algorithms, machine learning, and Alzheimer's disease.